From Wrinkles to Creases in Elastomers: The Instability and Imperfection-Sensitivity of Wrinkling

From wrinkles to creases in elastomers: The instability and imperfection-sensitivity of wrinkling

Yanping Cao [1] and John W. Hutchinson [2] *

[1] AML, Department of Engineering Mechanics
Tsinghua University, 100084, Beijing, P. R. China
[2] School of Engineering and Applied Sciences
Harvard University, Cambridge, MA 02138 USA

Abstract

The stability of the wrinkling mode experienced by a compressed half-space of neo-Hookean material is investigated using analytical and numerical methods to study the post-bifurcation behavior of periodic solutions. It is shown that wrinkling is highly unstable due to the nonlinear interaction among the multiple modes associated with the critical compressive state. Concomitantly, wrinkling is sensitive to exceedingly small initial imperfections that significantly reduce the compressive strain at which the instability occurs. The study provides insight into the connection between wrinkling and an alternative surface mode, the finite amplitude crease, or sulcus. The shape of the critical combination of wrinkling modes has the form of an incipient crease, and a tiny initial imperfection can trigger a wrinkling instability that collapses into a crease.

Keywords: wrinkling, creasing, instability, imperfection-sensitivity, neo-Hookean elasticity

*Author for correspondence (hutchinson@husm.harvard.edu)

1. Introduction

Surface instabilities are frequently observed when highly elastic soft materials are compressed (Gent & Cho 1999; Tanaka et al. 1987; Trujillo et al. 2008; Cai, Chen et al. 2011) and their importance has grown along with the steady increase in applications of soft materials (Soft Matter, November 2010). Biot (1963, 1965) appears to be the first to have demonstrated the existence of wrinkling instability modes at the surface of an incompressible neo-Hookean elastic half-space. These modes occur as a bifurcation from a state of uniform compression with the unusual feature that their wavelength is undetermined—the scale of wrinkle undulations is arbitrary as long as it is short compared to any other geometric dimension of the solid. Throughout this paper, the coordinate x_1 is aligned with the direction of in-plane compression, x_2 is aligned perpendicular to the free surface of the undeformed half-space, and x_3 is the out-of-plane coordinate (Fig.1). The stretches in the uniform pre-bifurcation state are denoted by λ_1, λ_2 and λ_3. With λ_3 imposed and fixed, Biot found that bifurcation into in-plane wrinkling modes occurs when the in-plane compression attains

$$\lambda_1 / \lambda_2 = 0.2956 \quad \text{or} \quad \lambda_1 = \lambda_W \equiv 0.5437 / \sqrt{\lambda_3} \tag{1.1}$$

The crease, or sulcus, surface mode, first analyzed by Hohlfeld (2008) and Hohlfeld & Mahadevan (2011), is doubly unusual in that, in addition to having arbitrary wavelength, or depth, it does not emerge as a bifurcation but rather exists as a local state involving a finite strain changes from the uniform compressive state. By carrying out a finite element analysis of this state in a neo-Hookean half-space, Hong et al. (2009) have shown that for any fixed λ_3 a crease is energetically favorable for compression in the fundamental state exceeding

$$\lambda_1 / \lambda_2 = 0.42 \quad \text{or} \quad \lambda_1 = \lambda_C \equiv 0.65 / \sqrt{\lambda_3} \tag{1.2}$$

A crease will lower the energy of the solid when the compressive strain exceeds (1.2), but the deformation pathway leading to crease formation was not determined by these authors. The mystery underlying these two modes is heightened by the fact that a crease can exist at smaller compressive (nominal) strain than that required for the onset of wrinkling, i.e.,

$$\varepsilon_C = 1-\lambda_C = 1-0.65/\sqrt{\lambda_3} \quad \text{vs.} \quad \varepsilon_W = 1-\lambda_W = 1-0.5437/\sqrt{\lambda_3}$$

Hohlfeld and Mahadevan (2011) explored the closing and opening pathways of a finite amplitude crease under a cycle of applied compression by attaching a very thin film with bending stiffness to the surface whose purpose is to regularize the numerical model by fixing the wavelength. As these authors emphasize, the free surface of any soft elastic solid is susceptible to wrinkling and creasing under compression because the mode wavelengths can be arbitrarily small and locally a surface will be effectively flat.

The present paper builds on the work cited above with a two-fold objective: to determine the stability of wrinkling by carrying out a nonlinear post-bifurcation analysis, and to account for the role of initial imperfections in the form of slight surface undulations on the stability of the wrinkles. A clear pathway to crease formation emerges. The paper is organized into sections as follows. Section 2 develops the energy functional for the neo-Hookean half-space on which the analysis is based, and it briefly reviews Biot's (1963, 1965) bifurcation results which form the starting point in the nonlinear analysis. In Section 3, Koiter's (1945, 2009) post-bifurcation approach is presented as relevant to wrinkling—the finite deformation of a nonlinear elastic solid with multiple modes associated with the critical bifurcation stress. The detailed analysis of stability and imperfection-sensitivity is executed in Section 4. The numerical analysis of the role of imperfections on the stability of wrinkling is presented in Section 5. Two types of imperfections are considered: a sinusoidal surface undulation in the shape of one of the classical wrinkling modes similar to that considered in the analytic study, and an isolated slight surface depression. The numerical analysis reveals connections between wrinkling and creasing which are summarized in the conclusions in Section 6.

2. Energy functional and the bifurcation solution

Let x_i, $i=1,3$ be Cartesian coordinates defined above labeling material points in the undeformed body (Fig.1). These coordinates will be used throughout the analysis. All tensor components will be referred to these coordinates. Let $u_i(\mathbf{x})$ be the displacements of the material points in the deformed state with the Lagrangian strain tensor, η_{ij}, defined by $2\eta_{ij} = (u_{i,j} + u_{j,i}) + u_{k,i}u_{k,j}$. Denote the stretches in the

fundamental uniform state by λ_i subject to a constraint of incompressibility, $\lambda_1\lambda_2\lambda_3 = 1$. The material points on the free surface are given by $x_2 = 0$ with a semi-infinite slab of neo-Hookean material below. An arbitrary uniform stretch λ_3 is allowed but, once imposed, it is held fixed. The non-uniform wrinkling deformations associated with bifurcation are restricted to satisfy plane strain conditions in the (x_1, x_2) plane. The applied load parameter is the stretch $\lambda \equiv \lambda_1$ associated with the uniform solution, i.e., the average stretch in the 1-direction, λ, is imposed with $\lambda_2 = \lambda_3 / \lambda_1$. Solutions which are periodic with wavelength, $l = 2\pi / k$, with respect to the reference x_1 coordinate are sought, having wavelength λl in the deformed state.

Let $\varphi(\boldsymbol{\eta})$ be the strain energy per unit volume of the strained material with μ as the ground state shear modulus. Let

$$\Phi = \int_V \left(\varphi(\boldsymbol{\eta}) - \varphi(\boldsymbol{\eta}^{(0)})\right) dV = \int_0^l dx_1 \int_{-\infty}^0 dx_2 \left(\varphi(\boldsymbol{\eta}) - \varphi(\boldsymbol{\eta}^{(0)})\right) \tag{2.1}$$

be the energy change/wavelength (per unit depth of undeformed material) relative to the imposed uniform state having strain $\boldsymbol{\eta}^{(0)}$ associated with imposed λ (and λ_3). Let $u_i^{(0)} = (\lambda_i - 1)x_i$ (no sum on i) be the displacements associated with the uniform solution and denote the total displacements by

$$u_i = u_i^{(0)}(\lambda) + U_i(x_1, x_2) \tag{2.2}$$

where the additional displacements U_i, $i = 1, 2$ are restricted to have the periodicity noted above with zero average stretch in the 1-direction. For a neo-Hookean material:

$$\varphi(\boldsymbol{\eta}) - \varphi(\boldsymbol{\eta}^{(0)}) = \mu\left(\lambda_1 U_{1,1} + \lambda_2 U_{2,2} + \tfrac{1}{2}\left({U_{1,1}}^2 + {U_{2,2}}^2 + {U_{1,2}}^2 + {U_{2,1}}^2\right)\right)$$

The incompressibility condition is $C(\lambda, U) = 0$ where

$$C(\lambda, U) = \lambda_2 U_{1,1} + \lambda_1 U_{2,2} + U_{1,1}U_{2,2} - U_{1,2}U_{2,1}$$

The modified energy functional, including a Lagrangian multiplier function, $q(x_1, x_2)$, to enforce incompressibility, is

$$\hat{\Phi} = \mu \int_V \left(\left(\lambda_1 U_{1,1} + \lambda_2 U_{2,2} + \tfrac{1}{2}\left({U_{1,1}}^2 + {U_{2,2}}^2 + {U_{1,2}}^2 + {U_{2,1}}^2\right)\right) - q\, C(\lambda, U)\right) dV \tag{2.3}$$

To eliminate the terms linear in U_i, let $q = r + Q(x_1, x_2)$ with $r \equiv \lambda_2 / \lambda_1$ where $Q(x_1, x_2)$ has the same periodicity as U_i; the linear terms in U_2 cancel. By periodicity, the term linear in $U_{1,1}$ integrates to zero. The modified functional becomes:

$$\hat{\Phi}(\lambda, U, Q) = \mu \int_V \left(I(\lambda, U, Q) \right) dV , \tag{2.4}$$

$$\begin{aligned} I(\lambda, U, Q) = {} & \tfrac{1}{2}\left({U_{1,1}}^2 + {U_{2,2}}^2 + {U_{1,2}}^2 + {U_{2,1}}^2 \right) - Q\left(\lambda_2 U_{1,1} + \lambda_1 U_{2,2} \right) \\ & - (r + Q)\left(U_{1,1} U_{2,2} - U_{1,2} U_{2,1} \right) \end{aligned} \tag{2.5}$$

At prescribed λ, conditions of equilibrium and incompressibility are given by the requirement that the first variations of $\hat{\Phi}$ with respect to U_i and Q vanish subject to periodicity and such that the overall stretch λ is not altered by U_i.

The lowest order terms in the functional are quadratic in the unknowns (U, Q). The eigenvalue problem for the critical stretch, λ_W, is the variational problem, $\delta \hat{\Phi} = 0$, based on the quadratic terms in (2.4) with (U, Q) and their variations restricted to have the periodicity noted earlier and to decay as $x_2 \to -\infty$. This is the Biot wrinkling problem which is briefly outlined below. The Euler equations for the problem are

$$\begin{aligned} & U_{1,11} + U_{1,22} - r\lambda_1 Q_{,1} = 0 \\ & U_{2,22} + U_{2,11} - \lambda_1 Q_{,2} = 0 \\ & r U_{1,1} + U_{2,2} = 0 \end{aligned} \tag{2.6}$$

with boundary conditions on $x_2 = 0$: $U_{1,2} + r U_{2,1} = 0$ and $2r U_{1,1} + \lambda_1 Q = 0$. This problem admits separated periodic solutions of the form

$$(U_1, U_2, \lambda_1 Q) = \left(f(kx_2) \sin kx_1, g(kx_2) \cos kx_1, kh(kx_2) \cos kx_1 \right) \tag{2.7}$$

The two characteristic solutions to (2.6), $\left(f(kx_2), g(kx_2), h(kx_2) \right) = \left(F, G, H \right) e^{ksx_2}$, which decay to zero as $x_2 \to -\infty$ have $s = r$ and $s = 1$, with $F = -G$, $H = Gr^{-1}(r^2 - 1)$ for $s = r$ and $F = -Gr^{-1}$, $H = 0$ for $s = 1$. Satisfaction of the boundary conditions on $x_2 = 0$ gives the eigenvalue condition

$$r^3 - 3r^2 - r - 1 = 0 \;\Rightarrow\; r = \lambda_2 / \lambda_1 = 3.3830 \tag{2.8}$$

and

$$f(\zeta) = (1-r^2)^{-1}\left(-(1+r^2)e^{r\zeta} + 2re^{\zeta}\right)$$
$$g(\zeta) = (1-r^2)^{-1}\left((1+r^2)e^{r\zeta} - 2r^2e^{\zeta}\right) \tag{2.9}$$
$$h(\zeta) = -r^{-1}(1+r^2)e^{r\zeta}$$

where the normalization $g(0)=1$ has been enforced. The solution holds for any wave number k and prescribed λ_3 with λ_W given by (1.1).

Multiple eigenmodes with the same periodicity exist associated with the critical stretch. To define them, identify the n^{th} mode in the set using the notation $U_i = u_i^{(n)}$ and $Q = q^{(n)}$. With $k = 2\pi / l$,

$$\left(u_1^{(n)}, u_2^{(n)}, \lambda_1 q^{(n)}\right) = l\left(f(nkx_2)\sin(nkx_1),\ g(nkx_2)\cos(nkx_1),\ nk\,h(nkx_2)\cos(nkx_1)\right) \tag{2.10}$$

for $n = 1, 2, 3, \ldots$. Here, the period, l, which is the only length scale in the problem, is employed as a dimensional normalizing factor. Attention has been restricted to modes that are symmetric about $x_1 = 0$. The normalization in (2.10) is such that on $x_2 = 0$ the modal displacement normal to the free surface is $u_2^{(n)} = l\cos(nkx_1)$.

In the analysis which follows, the total displacement will be expanded in the form

$$(u_i, q) = \left(u_i^0(\lambda), q^0(\lambda)\right) + \sum_{n=1}^{N} \xi_n \left(u_i^{(n)}, q^{(n)}\right) + \left(\Delta u_i, \Delta q_i\right) \tag{2.11}$$

with $q^0(\lambda) = r$ and ξ_n as the dimensionless amplitude of the n^{th} mode. Higher order terms in the expansion are denoted by $\left(\Delta u_i, \Delta q_i\right)$.

3. Koiter's initial post-bifurcation analysis for wrinkling

(a) The perfect system

In this section, a general result for the energy change in the vicinity of the bifurcation point will be derived using a compact notation. A general relation is sought between the prescribed overall stretch, λ, and the amplitudes of the bifurcation modes in the equilibrium post-bifurcation state which are denoted collectively by ξ. In the general notation, this relation has the form

$$\lambda = \lambda_W\left(1 + a\xi + b\xi^2 + \ldots\right) \tag{3.1}$$

For wrinkling it turns out that $a \neq 0$ and it will not be necessary to obtain b because it will be seen that $a \neq 0$ already implies that the bifurcation solution is highly unstable. With reference to the expansion (2.11), the bifurcation modes are represented collectively as

$$\xi U^{(1)} = \sum_{n=1}^{N} \xi_n \left(u_i^{(n)}, q^{(n)} \right)$$

In the same compact notation, let $\xi^2 U^{(2)}$ denote all the terms that are quadratic in the amplitudes of the bifurcation modes. In this compact notation, the initial post-bifurcation expansion takes the form

$$U = U_0(\lambda) + \xi U^{(1)} + \xi^2 U^{(2)} + ... \equiv U_0(\lambda) + \tilde{U} \tag{3.2}$$

The modified energy functional (2.4) is denoted by $\hat{\Phi}(\lambda, \tilde{U})$. Equilibrium in the bifurcated state and the constraint on volume change requires satisfaction of the variational equation

$$\delta \hat{\Phi} = \frac{\partial \hat{\Phi}(\lambda, \tilde{U})}{\partial \tilde{U}} \delta U \equiv \int_V \left\{ \frac{\partial I(\lambda, U, Q)}{\partial U_{i,j}} \delta U_{i,j} + \frac{\partial I(\lambda, U, Q)}{\partial Q} \delta Q \right\} dV = 0$$

for all admissible $\delta U \equiv (\delta U_i, \delta Q)$ satisfying periodicity with no average stretch. Expand this condition about $(\lambda_C, 0)$, noting that $\left[\partial \hat{\Phi}(\lambda, \tilde{U}) / \partial \tilde{U} \right]_{\tilde{U}=0} = 0$ and $\left[\partial^2 \hat{\Phi}(\lambda, \tilde{U}) / \partial \lambda \partial \tilde{U} \right]_{\tilde{U}=0} = 0$, obtaining

$$\frac{\partial \hat{\Phi}(\lambda, \tilde{U})}{\partial \tilde{U}} \delta U = \left[\frac{\partial^2 \hat{\Phi}(\lambda_W, 0)}{\partial^2 \tilde{U}} + \frac{\partial^3 \hat{\Phi}(\lambda_W, 0)}{\partial \lambda \partial^2 \tilde{U}} \lambda_W a \xi + ... \right] \left[\xi U^{(1)} + \xi^2 U^{(2)} + ... \right] \delta U +$$

$$+ \frac{1}{2} \frac{\partial^3 \hat{\Phi}(\lambda_W, 0)}{\partial^3 \tilde{U}} \left[\xi U^{(1)} + \xi^2 U^{(2)} + ... \right]^2 \delta U \ + ... = 0$$

with notation such as $\left[\partial^2 \hat{\Phi}(\lambda_W, \tilde{U}) / \partial^2 \tilde{U} \right]_{\tilde{U}=0} = \partial^2 \hat{\Phi}(\lambda_W, 0) / \partial^2 \tilde{U}$. In increasing powers of ξ, this becomes

$$\frac{\partial\hat{\Phi}(\lambda,\tilde{U})}{\partial\tilde{U}}\delta U=\xi\left[\frac{\partial^2\hat{\Phi}(\lambda_w,0)}{\partial^2\tilde{U}}U^{(1)}\delta U\right]+$$
$$+\xi^2\left[\frac{\partial^2\hat{\Phi}(\lambda_w,0)}{\partial^2\tilde{U}}U^{(2)}\delta U+a\lambda_w\frac{\partial^3\hat{\Phi}(\lambda_w,0)}{\partial\lambda\partial^2\tilde{U}}U^{(1)}\delta U+\frac{1}{2}\frac{\partial^3\hat{\Phi}(\lambda_w,0)}{\partial^3\tilde{U}}U^{(1)2}\delta U\right] \quad (3.3)$$
$$+O\xi^3\ =0$$

The eigenvalue problem governing bifurcation solved earlier is obtained by setting the terms of order ξ to zero for all admissible δU, i.e.,

$$\frac{\partial^2\hat{\Phi}(\lambda_w,0)}{\partial^2\tilde{U}}U^{(1)}\delta U=0$$

Each of the higher terms in the expansion, $U^{(m)}$, is admissible and, thus,

$$\frac{\partial^2\hat{\Phi}(\lambda_w,0)}{\partial^2\tilde{U}}U^{(1)}U^{(m)}=\frac{\partial^2\hat{\Phi}(\lambda_w,0)}{\partial^2\tilde{U}}U^{(m)}U^{(1)}=0\ ,\ m=1,2,... \quad (3.4)$$

The variational problem for $U^{(2)}$ is obtained from the terms of order ξ^2:

$$\frac{\partial^2\hat{\Phi}(\lambda_w,0)}{\partial^2\tilde{U}}U^{(2)}\delta U=-a\lambda_w\frac{\partial^3\hat{\Phi}(\lambda_w,0)}{\partial\lambda\partial^2\tilde{U}}U^{(1)}\delta U-\frac{1}{2}\frac{\partial^3\hat{\Phi}(\lambda_w,0)}{\partial^3\tilde{U}}U^{(1)2}\delta U$$

(Orthogonality conditions on $U^{(2)}$ relative to $U^{(1)}$ must also be imposed if one solves for $U^{(2)}$, but this will not be necessary.) With $\delta U=U^{(1)}$ in the above equation and use of (3.1), one obtains the compact equation for the bifurcation coefficient, a:

$$a\lambda_w\frac{\partial^3\hat{\Phi}(\lambda_w,0)}{\partial\lambda\partial^2\tilde{U}}U^{(1)2}=-\frac{1}{2}\frac{\partial^3\hat{\Phi}(\lambda_w,0)}{\partial^3\tilde{U}}U^{(1)3} \quad (3.5)$$

For most problems, this condition gives $a=0$, but for the wrinkle problem with multiple modes we will find $a\neq 0$ and it is not necessary to proceed further. Detailed information on mode coupling will also emerge.

The above results can be used to express the energy change, $\hat{\Phi}(\lambda,\tilde{U})$, from the fundamental state. Because $\hat{\Phi}(\lambda,0)=0$ and $\partial\hat{\Phi}(\lambda,0)/\partial\tilde{U}=0$, it also follows that

$$\frac{\partial\hat{\Phi}(\lambda,0)}{\partial\lambda}=0,\ \ \frac{\partial^2\hat{\Phi}(\lambda,0)}{\partial\lambda\partial\tilde{U}}=0,\ \textit{etc.}$$

Using expansions for λ and U, making use of the above, one finds

$$\hat{\Phi}(\lambda,U)=\frac{1}{2}\left[\frac{\partial^2\hat{\Phi}(\lambda_w,0)}{\partial^2\tilde{U}}+\frac{\partial^3\hat{\Phi}(\lambda_w,0)}{\partial\lambda\partial^2\tilde{U}}(\lambda-\lambda_w)+...\right]\left[\xi U^{(1)}+\xi^2U^{(2)}+....\right]^2+$$
$$+\frac{1}{6}\left[\frac{\partial^3\hat{\Phi}(\lambda_w,0)}{\partial^3\tilde{U}}+\frac{\partial^4\hat{\Phi}(\lambda_w,0)}{\partial\lambda\partial^3\tilde{U}}(\lambda-\lambda_w)+...\right]\left[\xi U^{(1)}+\xi^2U^{(2)}+....\right]^3+.....=0$$

Accounting for the terms that vanish by virtue of the eigenvalue problem, gives

$$\hat{\Phi}(\lambda,U)=\frac{1}{2}(\lambda-\lambda_w)\xi^2\frac{\partial^3\hat{\Phi}(\lambda_w,0)}{\partial\lambda\partial^2\tilde{U}}U^{(1)2}+\frac{1}{6}\xi^3\frac{\partial^3\hat{\Phi}(\lambda_w,0)}{\partial^3\tilde{U}}U^{(1)3}$$
$$+O(\xi^4,(\lambda-\lambda_w)\xi^3) \qquad (3.6)$$

Equation (3.6) allows one identify the expression for $\frac{1}{6}\frac{\partial^3\hat{\Phi}(\lambda_w,0)}{\partial^3\tilde{U}}\tilde{U}^3$ as the cubic terms in U from (2.4) and (2.5), i.e.,

$$\frac{1}{6}\frac{\partial^3\hat{\Phi}(\lambda_w,0)}{\partial^3\tilde{U}}U^3=\frac{\mu}{\lambda_1}\int_V I_3(\lambda,U,Q)\,dV \qquad (3.7)$$

with

$$I_3(\lambda,U,Q)=-\left(\lambda_1 Q\right)\left(U_{1,1}U_{2,2}-U_{1,2}U_{2,1}\right)$$

Based on the quadratic terms in (2.4) and noting $\partial\lambda_2/\partial\lambda=-r$ and $\partial r/\partial\lambda=-2r/\lambda_1$, it is also straightforward to obtain

$$\frac{1}{2}\frac{\partial^3\hat{\Phi}(\lambda_w,0)}{\partial\lambda\partial^2\tilde{U}}U^2=\frac{\mu}{\lambda_1}\int_V\left\{\left(\lambda_1 Q\right)\left(rU_{1,1}-U_{2,2}\right)+2r\left(U_{1,1}U_{2,2}-U_{1,2}U_{2,1}\right)\right\}dV \qquad (3.8)$$

In (3.7) and (3.8), λ_1 and r are evaluated at λ_w.

(b) The imperfect system—lowest order contribution of a geometric imperfection

A slight imperfection in the form of a periodic undulation of the surface of the undeformed half-space is assumed:

$$x_2=\delta(x_1)=\sum_{n=1}^{N}\bar{\xi}_n l\cos(nkx_1) \qquad (3.9)$$

with $\bar{\xi}_n$ as the amplitude of the imperfection in the n^{th} mode.

The objective is to obtain asymptotic results for the effect of very small imperfections on behavior in the vicinity of the bifurcation point and, in particular, on the occurrence of

the wrinkling instability. Only the lowest order influence of the imperfections is sought following an approach similar to that of Koiter (1945, 2009).

For the initial undulation, Φ in (2.1) can be written as

$$\Phi = \int_0^l dx_1 \int_{-\infty}^0 dx_2 \left(\varphi(\boldsymbol{\eta}) - \varphi(\boldsymbol{\eta}^{(0)})\right) + \int_0^l dx_1 \int_0^{\delta(x_1)} dx_2 \left(\varphi(\boldsymbol{\eta}) - \varphi(\boldsymbol{\eta}^{(0)})\right) \tag{3.10}$$

For very small $\delta(x_1)$,

$$\int_0^{\delta(x_1)} dx_2 \left(\varphi(\boldsymbol{\eta}) - \varphi(\boldsymbol{\eta}^{(0)})\right) \cong \delta(x_1)\left(\varphi(\boldsymbol{\eta}) - \varphi(\boldsymbol{\eta}^{(0)})\right)_{x_2=0},$$

such that the lowest order contribution to $\hat{\Phi}$ due to the imperfection is

$$\Delta\Phi = \int_0^l dx_1 \int_0^{\delta(x_1)} dx_2 \left(\varphi(\boldsymbol{\eta}) - \varphi(\boldsymbol{\eta}^{(0)})\right) \cong \int_0^l \delta(x_1)\left(\varphi(\boldsymbol{\eta}) - \varphi(\boldsymbol{\eta}^{(0)})\right)_{x_2=0} dx_1 \tag{3.11}$$

Then, note that

$$\left(\varphi(\boldsymbol{\eta}) - \varphi(\boldsymbol{\eta}^{(0)})\right)_{x_2=0} = \left(\frac{\partial\varphi(\boldsymbol{\eta}^{(0)})}{\partial\eta_{ij}}\Delta\eta_{ij} + \ldots\right)_{x_2=0} = \left(\tau_{ij}^0\Delta\eta_{ij} + \ldots\right)_{x_2=0} \tag{3.12}$$

where, to lowest order in U_i, $2\Delta\eta_{ij} = (U_{i,j} + U_{j,i}) + u_{k,i}^0 U_{k,j} + u_{k,j}^0 U_{k,i}$, and $\tau_{ij}^0(\lambda)$ is the Piola-Kirchhoff stress in the fundamental state. With $\tau_{11}^0 = -\mu(r^2 - 1)$, the lowest order contribution of the imperfection to $\hat{\Phi}$ is

$$\Delta\Phi = -\mu\lambda_1 l(r-1)^2 \int_0^l \left(\delta(x_1)\sum_{n=1}^N \xi_n u_{1,1}^{(n)}(x_1, 0)\right) dx_1 \tag{3.13}$$

4. The instability of wrinkling

(a) Evaluation of the post-buckling coefficients

In the notation of (2.10) and (3.2), we consider the first N modes:

$$\xi U^{(1)} = \sum_{n=1}^N \xi_n \left(u_1^{(n)}, u_2^{(n)}, \lambda_1 q^{(n)}\right) \tag{4.1}$$

A direct evaluation of the integral in (3.8) gives

$$\frac{1}{2}\xi^2 \frac{\partial^3\hat{\Phi}(\lambda_W, 0)}{\partial\lambda\partial^2\tilde{U}} U^{(1)2} = \frac{\mu l^2 A}{\lambda_W}\sum_{n=1}^N n\xi_n{}^2, \qquad A = 9.3438 \tag{4.2}$$

while (3.7) gives

$$\frac{1}{6}\xi^3\frac{\partial^3\hat{\Phi}(\lambda_W,0)}{\partial^3\tilde{U}}U^{(1)3}=\frac{\mu l^2A}{\lambda_W}\Big(b_{112}\xi_1{}^2\xi_2+b_{123}\xi_1\xi_2\xi_3+b_{224}\xi_2{}^2\xi_4+b_{134}\xi_1\xi_3\xi_4 \\ +b_{235}\xi_2\xi_3\xi_5+b_{145}\xi_1\xi_4\xi_5+b_{156}\xi_1\xi_5\xi_6+b_{246}\xi_2\xi_4\xi_6+b_{336}\xi_3{}^2\xi_6\ \Big) \tag{4.3}$$

with

$$b_{112}=b_{224}/4=b_{336}/9=2.4792,\quad b_{123}=b_{246}/4=9.6303,$$
$$b_{134}=13.882,\ b_{235}=29.445,\ b_{145}=17.886,\ b_{156}=21.735$$

Coefficients for $N=6$ are listed but some results below have been computed with N as large as 10. The nonlinear coupling of modes 1 and 2 is illustrated by the cubic term, $b_{112}\xi_1{}^2\xi_2$, in (4.3). It arises due to the fact that products of quadratic terms from mode 1, proportional to $\cos(kx_1)^2=(1+\cos(2kx_1))/2$, and linear terms from mode 2, proportional to $\cos(2kx_1)$, are not orthogonal. On the other hand, the phasing of cubic terms proportional to $\xi_1{}^3$, $\xi_2{}^3$ and $\xi_1\xi_2{}^2$ is such that they integrate to zero.

The contribution (3.13) from the initial imperfection is

$$\Delta\Phi=-17.8405\mu\lambda_1l^2\sum_{n=1}^{N}n\bar{\xi}_n\xi_n\equiv-\frac{\mu l^2A}{\lambda_W}2c\lambda_W{}^2\sum_{n=1}^{N}n\bar{\xi}_n\xi_n \tag{4.4}$$

with $c=0.95467$.

(b) The post-bifurcation equations

The modified energy functional in (3.6) plus the contribution due to the imperfection is (illustrated for $N=6$)

$$\frac{\hat{\Phi}(\lambda,U,\bar{\xi})}{\mu l^2A/\lambda_W}=(\lambda-\lambda_W)\sum_{i=1}^{N}n\xi_n{}^2-2c\lambda_W{}^2\sum_{i=1}^{N}n\bar{\xi}_n\xi_n+b_{112}\xi_1{}^2\xi_2+b_{123}\xi_1\xi_2\xi_3+b_{224}\xi_2{}^2\xi_4 \\ +b_{134}\xi_1\xi_3\xi_4+b_{235}\xi_2\xi_3\xi_5\ +b_{145}\xi_1\xi_4\xi_5+b_{156}\xi_1\xi_5\xi_6+b_{246}\xi_2\xi_4\xi_6+b_{336}\xi_3{}^2\xi_6 \\ +O(\xi^4,\bar{\xi}\xi^2,\bar{\xi}^2\xi) \tag{4.5}$$

This result holds for any prescribed value of λ_3, with λ_W given by (1.1). Equilibrium requires $\partial\hat{\Phi}/\partial\xi_i=0$ for $i=1,N$. For $N=6$, the equations are:

$$2(\lambda-\lambda_W)\xi_1+2b_{112}\xi_1\xi_2+b_{123}\xi_2\xi_3+b_{134}\xi_3\xi_4+b_{145}\xi_4\xi_5+b_{156}\xi_5\xi_6=2c\lambda_W{}^2\bar{\xi}_1$$
$$4(\lambda-\lambda_W)\xi_2+b_{112}\xi_1{}^2+b_{123}\xi_1\xi_3+2b_{224}\xi_2\xi_4+b_{235}\xi_3\xi_5+b_{246}\xi_4\xi_6=4c\lambda_W{}^2\bar{\xi}_2$$
$$6(\lambda-\lambda_W)\xi_3+b_{123}\xi_1\xi_2+b_{134}\xi_1\xi_4+b_{235}\xi_2\xi_5+2b_{336}\xi_3\xi_6=6c\lambda_W{}^2\bar{\xi}_3 \tag{4.6}$$

$$8(\lambda-\lambda_W)\xi_4+b_{224}\xi_2{}^2+b_{134}\xi_1\xi_3+b_{145}\xi_1\xi_5+b_{246}\xi_2\xi_6=8c\lambda_W{}^2\overline{\xi}_4$$

$$10(\lambda-\lambda_W)\xi_5+b_{235}\xi_2\xi_3+b_{145}\xi_1\xi_4+b_{156}\xi_1\xi_6=10c\lambda_W{}^2\overline{\xi}_5$$

$$12(\lambda-\lambda_W)\xi_6+b_{156}\xi_1\xi_5+b_{246}\xi_2\xi_4+b_{336}\xi_3{}^2=12c\lambda_W{}^2\overline{\xi}_6$$

These relations are asymptotically valid in the vicinity of the bifurcation point for sufficiently small imperfections.

(c) Post-bifurcation solutions—the perfect system

The two-mode approximation: Setting all the mode amplitudes to zero in (4.6) except for the first two modes and their imperfections, one has

$$\begin{aligned}&\left(\lambda-\lambda_W\right)\xi_1+b_{112}\xi_1\xi_2=c\lambda_W{}^2\overline{\xi}_1\\&\left(\lambda-\lambda_W\right)\xi_2+b_{112}\,\xi_1{}^2/4=c\lambda_W{}^2\overline{\xi}_2\end{aligned}\qquad(4.7)$$

For the perfect system ($\overline{\xi}_1=\overline{\xi}_2=0$), the solutions of interest are

$$\xi_1=\pm2(\lambda-\lambda_W)/b_{112},\quad \xi_2=-\left(\lambda-\lambda_W\right)/b_{112},\quad \text{with } \lambda-\lambda_W\geq0\qquad(4.8)$$

In what follows it will be evident why the solutions of interest are those associated with *overall compressive strains less than the bifurcation value* (*i.e.*, $\lambda-\lambda_W\geq0$ or, equivalently, $\varepsilon-\varepsilon_W\leq0$ with $\varepsilon=1-\lambda$ as the compressive strain). The solutions are shown in Fig. 2. The existence of the non-zero cubic term, $b_{112}\xi_1{}^2\xi_2$, implies that *wrinkling bifurcation is unstable* at $\lambda=\lambda_W$ because the energy change on the equilibrium path relative to the bifurcation state,

$$\frac{\hat{\Phi}(\lambda_W,U)}{\mu l^2A/\lambda_W}=b_{112}\xi_1{}^2\xi_2=-0.651\left(\lambda-\lambda_W\right)^3,$$

is negative. The shape of surface wrinkle for the combined two-mode approximation,

$$u_2(x_1,0)=\frac{(\lambda-\lambda_W)l}{b_{112}}\left(2\cos(2\pi x_1/l)-\cos(4\pi x_1/l)\right),$$

is plotted in Fig.3. The wrinkle displays a deep-pronged penetration of the free surface into the material with relatively flat broad crests on either side.

N-mode approximations: By including the 3rd mode in (4.6), one sees that the 2-mode solution is indeed only an approximation—the term $b_{123}\xi_1\xi_2$ in the 3rd equation

requires non-zero ξ_3. A finite number of modes can only generate an approximate solution to the order considered because the modes in the infinite set are all coupled through the quadratic terms in the equilibrium equations.

For a given N, the solution to the system (4.6) has the form $\xi_n = \alpha_n(\lambda - \lambda_W)$ for $n = 1, N$ and, thus, the normalized surface undulation, $u_2(x_1, 0)/[(\lambda - \lambda_W)l]$ in Fig. 3 is independent of $(\lambda - \lambda_W)$ to the order considered in this paper. While any shape is possible according to the bifurcation solution, the post-bifurcation analysis identifies a definite shape, assuming periodicity. The normalized shape of the wrinkle at the surface in Fig. 3 has been determined by a sequence of calculations, each with N modes, for N ranging from 2 to 10. A standard numerical iterative algorithm for solving systems of coupled nonlinear algebraic equations was used to generate the α_n. The solution for the system of $N-1$ equations was employed as the initial guess in the iteration for the solution for the system with N equations, thereby leading to the regular progression of shape approximations shown.[1] The sequence is trending towards an incipient crease-like shape as more and more terms in the approximation are considered, although the shape for $N = 10$ does not yet appear to have converged.

(d) Post-bifurcation solutions—the imperfect system

The 2-mode approximation: Explicit results for the reduction of the compressive strain at which wrinkling becomes unstable are now given for an imperfection in the first mode ($\overline{\xi}_1 \neq 0$, $\overline{\xi}_2 = 0$). The second of (4.7) gives $\xi_2 = -b_{112}\xi_1^2/[4(\lambda - \lambda_W)]$. Substituting this into the first of (4.7), one finds $(\lambda - \lambda_W)\xi_1 - b_{112}{}^2\xi_1^3/[4(\lambda - \lambda_W)] = c\lambda_W{}^2\overline{\xi}_1$, which provides the relation between λ and ξ_1. Denote the minimum of λ (i.e., the maximum compressive strain in the presence of the imperfection) by λ^*; it is associated with $d\lambda/d\xi_1 = 0$ (see Fig. 2). Solving for $\lambda^* - \lambda_W$, one finds

[1] The nonlinear algebraic equations for the perfect system (4.6) admit other solutions. For example, period doubling can be illustrated by taking modes 2 and 4 as dominant and allowing for bifurcation in mode 1 or by including a small imperfection in mode 1.

$$\lambda^* - \lambda_W = \lambda_W \sqrt{\frac{3\sqrt{3}\, b_{112} c \left|\overline{\xi}_1\right|}{4}} = 1.7534 \lambda_W \sqrt{\left|\overline{\xi}_1\right|} \tag{4.9}$$

The stretch λ^* for the imperfect system corresponds to the maximum compressive overall strain on the equilibrium path. The solution at λ^* is unstable in the sense that it would snap dynamically and undergo a finite deformation into another configuration—almost certainly to a fully developed crease as will be seen later.

The effect of very small imperfections in lowering the compressive strain at which wrinkling becomes unstable is dramatic due to the fact it is proportional to $\sqrt{\overline{\xi}_1}$, as seen in Figs. 2 and 4. The type of nonlinear coupling among simultaneous modes in wrinkling is rare but it is similar to that in two structural problems that also have multiple buckling modes and are notoriously imperfection-sensitive—the elastic buckling of cylindrical shells under axial compression (Koiter 1945, 2009) and spherical shells under external pressure (Hutchinson 1967).

N-mode approximations: Consider again the half-space with an initial imperfection in the 1st mode , $\overline{\xi}_1 \neq 0$, with $\overline{\xi}_n = 0$ for $n > 1$. As in the perfect case, a sequence of calculations has been made with an increasing number of modes in the approximation. For any N, the solution to (4.6) at the point of the maximum overall compressive strain has the form $\lambda^* - \lambda_W = c^* \lambda_W \sqrt{\overline{\xi}_1}$ and $\xi_n = c_n \sqrt{\overline{\xi}_1}$. The coefficient c^* is given in Table 1, and the results for the reduction in the compressive stretch, $\lambda^* - \lambda_W$, at which wrinkling becomes unstable is plotted as a function of the imperfection amplitude in Fig. 4 for N ranging from 2 to 6. The results appear to be converging to a curve slightly above that for $N = 6$. The formula (4.9) based on the 2-mode approximation underestimates the reduction in the compressive strain at the wrinkling instability by about 35%.

Modes in approximation	$N = 2$	$N = 3$	$N = 4$	$N = 5$	$N = 6$
c^*: (i) max overall strain	1.754	2.077	2.226	2.305	2.358
c^* : (ii) $\varepsilon_A = \varepsilon_W$	2.133	2.227	2.336	2.379	2.408

Table 1. Imperfection-sensitivity coefficient based on two criteria.

With $\xi_n = \alpha_n(\lambda - \lambda_W)$ for $n = 1, N$ as the N-mode solution for the perfect system in (4.6), consider an *imperfection in the shape of the solution for the perfect system*, i.e., $\bar{\xi}_n = \alpha_n \bar{\xi}$ for $n = 1, N$, with $\bar{\xi}$ as the single imperfection amplitude. With $\xi_n = \alpha_n \xi$ for $n = 1, N$, it is straightforward to show that each of N equilibrium equations (4.6) reduces to the same equation: $(\lambda - \lambda_W)\xi - \xi^2 = c\lambda_W{}^2 \bar{\xi}$. The maximum compressive strain that can be imposed prior to instability is given by

$$\lambda^* - \lambda_W = 2\lambda_W \sqrt{c\bar{\xi}} = 1.9541 \lambda_W \sqrt{\bar{\xi}} \tag{4.10}$$

The imperfection-sensitivity implied by this result is similar to that predicted for an imperfection in the shape of the 1st mode.

An alternative instability condition for the imperfect half-space will be discussed in connection with the numerical solutions presented in the next section.

5. Plane strain finite element simulations of a half-space with initial imperfections

Two types of initial surface imperfections have been considered in the numerical simulations; a sinusoidal imperfection, $\delta(x_1) = \bar{\xi}_1 l \cos(2\pi x_1 / l)$, and a periodic array of non-interacting initial exponential depressions of the surface specified by

$$\delta(x_1) = -4\bar{\xi} l \, e^{-(x_1/l)^2} \tag{5.1}$$

A finite element mesh conforming to the initial surface undulation was created on a rectangular region in the (x_1, x_2) plane of width L and depth $D = 10L$ for the sinusoidal imperfection. The surface is traction-free, while the shear traction and u_2 are taken to be zero on the bottom surface. The depth is sufficient to ensure that the boundary conditions on the bottom have no influence on the wrinkling behavior. For the sinusoidal imperfection, periodic boundary condition are imposed on the vertical sides of the region and L is taken to be l. For the exponential imperfection (5.1), periodic boundary conditions on the sides are also assumed for computational convenience. The imperfection is located within the center of the region and L is chosen to be $20l$ with $D = 10l$ so as to ensure that there is essentially no interaction between neighboring

imperfections or the bottom—the results for this case can be regarded as that of an isolated imperfection of the form (5.1).

Plane strain ($\lambda_3 = 1$) finite element simulations are performed via the commercial software, ABAQUS (2008). Considering that the instability and the wrinkling-creasing transition occur at the central region of the upper surface, a very fine mesh is used in this region with a ratio of l to the element size taken to be approximately 2000. In the finite element simulations, the incompressible neo-Hookean material model is employed (ABAQUS, 2008). The hybrid element (CPE6MH) suitable for simulations of incompressible materials is adopted. To introduce the initial surface imperfections, finite element simulations are first run by specifying the boundary conditions ($u_2 = \bar{\xi}_1 l \cos(2\pi x_1 / l)$, $u_1 = 0$) on the upper surface for the sinusoidal imperfection and ($u_2 = -4\bar{\xi} l\, e^{-(x_1/l)^2}$, $u_1 = 0$) for the exponential imperfection. The function *IMPERFECTION in ABAQUS (2008) converts the displacements from this step to an initial stress-free geometric imperfection. This procedure is equivalent to directly meshing a block of stress-free material with the initial surface undulation. Simulations are performed to track the occurrence of the local instability and the formation of a crease, as reported below. Self-contact interaction is defined for the upper surface of the block. When a local wrinkling instability occurs, the global matrix of the system may be singular and the Riks method, the commonly-used numerical method for dealing with limit points, will fail. In the present simulations, the pseudo-dynamic method has been adopted. A brief description of the key idea behind this nonlinear solution method is outlined as follows.

The nonlinear equations solved in a finite element analysis can be written as

$$\boldsymbol{\Xi}(\boldsymbol{u}) - \boldsymbol{\Omega} = 0 \tag{5.2}$$

where $\boldsymbol{\Xi}$ is a nonlinear function of $\boldsymbol{u}$, symbolizing the displacements of the nodes, and $\boldsymbol{\Xi}(\boldsymbol{u})$ and $\boldsymbol{\Omega}$ denote internal forces and applied loads at the nodes, respectively. The pseudo-dynamic method regularizes the unstable problem by adding volume-proportional damping to the model such that equation (5.2) becomes

$$\boldsymbol{\Xi}(\boldsymbol{u}) - \boldsymbol{\Omega} + \boldsymbol{F}_v = 0 \tag{5.3}$$

where

$$\boldsymbol{F}_v = c\boldsymbol{M}\boldsymbol{v} \tag{5.4}$$

Here, $\boldsymbol{M}$ is an artificial mass matrix calculated with unity density, c is a damping factor, $\boldsymbol{v} = \Delta\boldsymbol{u}/\Delta t$ is the vector of nodal velocities, and Δt is the increment of time. When the model is stable (quasi-static), viscous forces and viscous energy dissipation are very small such that the artificial damping does not perturb the solution significantly. When the structure goes dynamically unstable, however, nodal velocities increase and, consequently, part of the strain energy released is dissipated by the damping. In simulations of the wrinkling problem, pseudo-dynamic regularization, which is now a standard feature in ABAQUS (2008), allows solutions to be generated under prescribed overall compressive strain when the wrinkle becomes unstable and develops into a crease. The role played by the damping factor c here is similar to that of the regularization factor in the Tikhonov regularization method (Tikhonov & Arsenin 1977) which is widely used to deal with ill-posed inverse problems.

(a) Wrinkling instability for sinusoidal imperfections

Fig. 5 presents the overall compressive strain at the point of wrinkling instability, $\varepsilon^* = 1 - \lambda^*$, as a function of the imperfection amplitude, $\overline{\xi}_1$. Included in this figure is the local compressive strain parallel to the surface at the deepest point of the wrinkle, $\varepsilon_A = 1 - \lambda_A$. As will be discussed in more detail below, the imperfect half-space becomes unstable with the local strain at the deepest point attains the Biot wrinkling strain, i.e., $\varepsilon_A = \varepsilon_W$. The simulations presented in Fig. 5 again reveal the extraordinarily strong imperfection-sensitivity of the overall compressive strain at instability, ε^*. Moreover, the numerical results confirm the accuracy of asymptotic result, $\lambda^* - \lambda_W = c^* \lambda_W \sqrt{\overline{\xi}_1}$, which has been included in Fig. 5, for reductions in overall strains larger than 0.1. In particular, imperfections larger than about $\overline{\xi}_1 = 0.008$ reduce the overall strain at instability to below the level needed to sustain a crease in the perfect system, i.e. $\varepsilon^* < \varepsilon_C$. This is a tiny initial undulation with an amplitude less than 1% of its wavelength. The

crease that forms at this low value of ε^* is localized within the region of strain concentration at the bottom of the larger scale wrinkle.

Further details of the evolution of the instability are illustrated in Figs. 6 and 7 for the case $\overline{\xi}_1 = 0.005$. The difference in height between the highest and deepest points on the surface, Δu_2, increases monotonically as the instability develops. Fig. 6 displays the local compressive strain at the deepest point, ε_A, and the overall strain, ε, as functions of $\Delta u_2 / l$ up to the onset of instability. At the onset, $\varepsilon_A = \varepsilon_W$, as already noted, and the overall compressive strain attains its maximum, ε^*. Upon attaining the onset condition at A, a small scale wrinkle forms within a narrow region on either side of A (Fig. 7). This smaller-scale wrinkle evolves into a fully developed crease under conditions in which the overall strain remains essentially unchanged at ε^*. The wavelength of the small scale wrinkle is comparable to the size of the finite elements, but once the crease develops, the crease depth is large compared to element size, as seen in Fig. 7b. The crease relaxes the compressive strain in its vicinity as seen from the plot of the compressive strain at the surface as a function of horizontal distance from the crease in the deformed body in Fig. 8. For horizontal distances from the center-line of the crease less than about $2.3l_C$, the surface strain has been reduced below the creasing strain, $\varepsilon_C = 0.35$, and at greater distances the strain does not exceed the wrinkling strain $\varepsilon_W = 0.456$. The numerical simulations indicate that the characteristic point on the surface at which the strain attains ε_C is nearly coincident with the inflection point corresponding to the transition of the surface from being convex to concave. No attempt has been made to simulate behavior at overall compressive strains beyond ε^* which would drive the crease even deeper than that shown in Figs. 7 and 8 and possibly nucleate new wrinkles and creases. Such calculations have recently been performed and compared with experimental observations by Cai, Chen et al. (2011).

In connection with Fig. 6 it was noted that the onset of wrinkling instability is associated with (almost) simultaneous satisfaction of two conditions: (i) attainment of an maximum in the overall compressive strain, and (ii) $\varepsilon_A = \varepsilon_W$. The analytical modeling of wrinkling instability in Section 4d is based on condition (i). Motivated by the numerical

findings related to the role of condition (ii), the analytical approach in Section 4d has been used to compute the overall stretch λ^* at which the local wrinkling condition, $\varepsilon_A = \varepsilon_W$, is met at the deepest point of the wrinkle on the surface at $x_1 = l/2$. The details of this calculation will not be given because they involve only a minor extension of the analysis in Section 3. The result has precisely the same functional form, $\lambda^* - \lambda_W = c^* \lambda_W \sqrt{\xi_1}$, as in the case of condition (i), where, as before, the coefficient c^* depends on the number of modes, N, in the approximation. The coefficient is presented in Table 1 along with that computed earlier based on condition (i). According to the analytical approximation, the local wrinkling condition (ii) is attained slightly before the maximum overall strain is reached. However, the difference between the overall critical stretch λ^* from two conditions is nearly negligible when 6 modes are used in the calculation (see Table 1). Thus, both the analytical and numerical predictions indicate that the two conditions, (i) and (ii), are attained nearly simultaneously at the onset of wrinkling instability and crease formation.

(b) Wrinkle instability for exponential imperfections

Simulations with the exponential imperfection (5.1) have also been carried out with results presented in Fig. 9. Wrinkling instability and the formation of a crease again occurs when the local strain at the deepest point of the surface wrinkle attains ε_W. A slight local depression on the surface of the half-space reduces the overall strain at the wrinkling instability to levels similar to that seen for the sinusoidal imperfection, based on comparable values of the normalized imperfection amplitudes that have been defined.

6. Conclusions

The post-bifurcation analysis of Biot's wrinkling problem reveals that wrinkling is extremely unstable and highly imperfection-sensitive. Wrinkling is also seen to be one pathway to the finite amplitude creasing mode. Wrinkling is so unstable and imperfection-sensitive that well developed wrinkles are not likely to be observed—a slight wrinkle will become dynamically unstable and trigger the formation of a crease. In this sense, the crease can be regarded as the collapse state of a wrinkle. The

wrinkle/crease connection has an analog in the elastic buckling of cylindrical shells under axial compression and spherical shells under external pressure which, like wrinkling, are characterized by multiple bifurcation modes associated with the critical stress. Buckling of these shell structures is also so unstable and imperfection-sensitive (Koiter 2009; Hutchinson 1967) that their short wavelength bifurcation modes are almost never observed because they become unstable at very small amplitudes and snap dynamically into a collapse state. Buckling modes observed in the collapsed state of the shell typically have much larger wavelengths than those of the bifurcation modes. A few experiments have employed high speed cameras to captured the bifurcation modes right after they are triggered (Brush & Almorth 1975) or have used a mandrel to arrest the buckles immediately after they have formed (Carlsson et al. 1967).

In addition, these shell structure/loading combinations are so imperfection-sensitive that, of the large number of shells tested over many years, none has reached a buckling load greater than about 1/2 of the buckling load of the perfect shell when the radius to thickness ratios exceeds 1000. In this respect, as well, there may be a close analog to wrinkling/creasing, i.e., the imperfection-sensitivity of wrinkling may be so strong that the maximum compressive strain of any actual realization of an elastomer layer will always lie well below Biot's wrinkling strain (1.1) due to inevitable surface imperfections.

There is one important respect in which wrinkling of a uniform half-space differs from cylindrical and spherical shell buckling—the wrinkling wavelength is undetermined and can be arbitrarily small. In principle, a perfectly flat surface should reach the Biot wrinkling strain but in practice, as noted above, it seems reasonable to assume that imperfections will always be present at some scale to trigger creases at strains just above the creasing strain. As Hohlfeld and Mahadevan (2011) have noted, wrinkles and creases are always lurking to destabilize a smooth surface of a compressed elastomer because their scale can be arbitrarily small. Examples have been presented in this paper for both sinusoidal and isolated imperfections wherein small scale wrinkles form in the vicinity of the point on the surface of maximum compression—wrinkles within wrinkles—and then spontaneously collapse into a local crease. An open question concerns the lower limit on the size of these instabilities. A continuum representation such as the neo-Hookean

material, with the elastomer represented by a constitutive model having no material length dependence, provides no lower limit on the scale of the instabilities. Surface effects such as a stiff thin layer of oxidized material would provide a limit. Strain gradient strengthening associated with deformation gradients that become comparable to scale of the polymeric microstructure would also place a lower limit on the size of the instabilities, but such effects have not yet been quantified for elastomers.

Finally, we note that the unstable wrinkling behavior of the uniform neo-Hookean half-space is in sharp contrast to the highly stable wrinkling behavior of a system comprised of a thin stiff film bonded to compliant half-space substrate. The film/substrate system buckles into wrinkling modes at very small compressive strains (Allen 1969). These systems can be compressed well beyond the critical bifurcation strain with the buckled state remaining stable (Cai, Bried et al. 2011). It is not at all unusual for experimental systems to display stable wrinkling behavior at an overall compressive strain ten times the bifurcation strain. Imperfections play a secondary role in the behavior of these systems. It remains for future work to explore the full parameter space of film/substrate systems to uncover the range of parameters in which a transition occurs from the highly stable buckling behavior associated with very stiff films to the highly unstable behavior associated with wrinkling of the uniform half-space.

Acknowledgement

The authors acknowledge the input from a reviewer who suggested the form of the incompressibility condition used in this paper. An earlier version of the paper employed an equivalent but less compact expression. YPC acknowledges the financial support from Tsinghua University (2009THZ02122).

References

ABAQUS analysis user's manual, version 6.8, (2008).

Allen, H. G. 1969, Analysis and design of sandwich panels. Pergamon Press, New York.

Biot, M.A. 1963 Surface instability of rubber in compression. Appl. Sci. Res. **12**, 168-182.

Biot, M.A. 1965 *Mechanics of incremental deformation*. New York, US: Wiley.

Brush, D.O. & Almroth, B.O. 1975 *Buckling of bars, plates and shells*. New York, US: McGraw Hill.

Cai, S., Breid, D., Crosby, A.I., Suo, Z. & Hutchinson, J.W. 2011 Periodic patterns and energy states of buckled films on compliant substrates. *J. Mech. Phys. Solids* **59**, 1094-1114.

Cai, S., Chen, D., Suo, Z. & Hayward, R.C. 2011 Creasing instability of elastomer films. Submitted for publication.

Carlson, R.L., Sendelbeck, R.L. & Hoff, N.J. 1967 Experimental studies of the buckling of complete spherical shells. *Exp. Mech*. **7**, 281-288.

Gent, A.N. & Cho, I.S. 1999 Surface instabilities in compressed or bent rubber blocks. *Rubber Chemistry and Technology* **72**, 253-262.

Hohlfeld, E.B. 2008 Creasing, post-bifurcations, and the spontaneous breakdown of scale invariance. PhD thesis, Harvard University, Cambridge, MA, US.

Holfeld, E.B. & Mahadevan, L. 2011 Unfolding the sulcus. *Phys. Rev. Letters* **106**, 105702-1-4.

Hong, W., Zhao, X. & Suo, Z. 2009 Formation of creases on the surfaces of elastomers and gels. *App. Phys. Letters* **95**, 111901-1-3.

Hutchinson, J.W. 1967 Imperfection sensitivity of externally pressurized spherical shells. *J. Appl. Mech.* 48-55.

Koiter, W.T. 1945 *On the stability of elastic equilibrium* (in Dutch with English summary). Thesis Delft, H.J. Paris, Amsterdam. An English translation is available online: http://imechanica.org/node/1400 .

Koiter, W.T., 2009. *Elastic stability of solids and structures*. A.M. van der Heijden (Ed.), Cambridge, UK: Cambridge University Press.

Soft Matter **6** 2010 Theme issue: The physics of buckling.

Tanaka, T., Sun, S-T., Hirokawa, Y., Katayama, S., Kucera, J., Hirose, Y. & Amiya, T. 1987 Mechanical instability of gels at phase transformation. *Nature* **325**, 796-798.

Tikhonov, A. N., Arsenin, V. Y. 1977. Solutions *of Ill*-Posed Problems, John Wiley & *Sons*, New York.

Trujillo, V., Kim, J. & Hayward, R.C. 2008 Creasing instability of surface-attached hydrogels. *Soft Matter* **4**, 564-569.

Figures

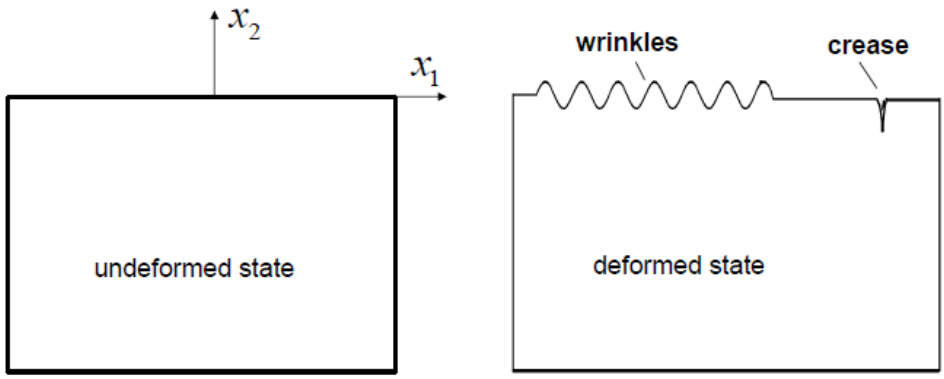

Fig. 1 Coordinates (x_1, x_2, x_3) identify locations of material points in the undeformed body. The pre-bifurcation deformation is characterized by uniform stretches $(\lambda_1, \lambda_2, \lambda_3)$ with $\lambda_1\lambda_2\lambda_3 = 1$. The bifurcation and post-bifurcation problems involve increments of displacement in the (x_1, x_2) plane with the out-of-plane stretch λ_3 held fixed.

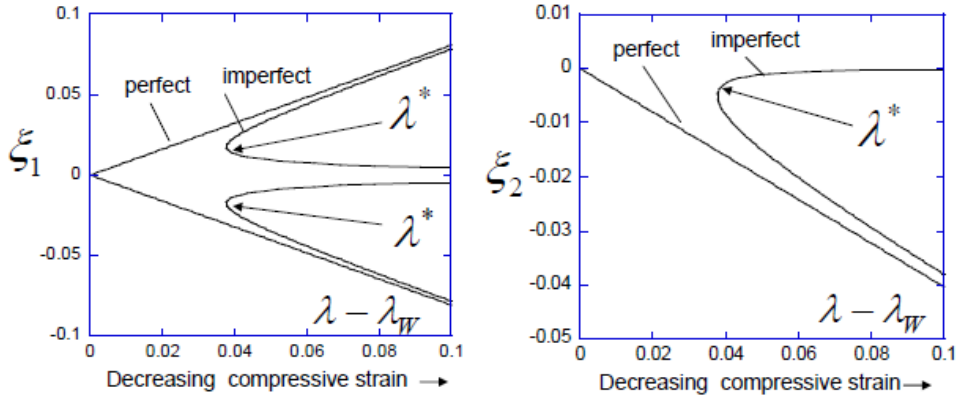

Fig. 2 Two-mode approximation for the post-bifurcation behavior of wrinkling for the perfect half-space ($\bar{\xi}_1 = \bar{\xi}_2 = 0$) and for a half space with slight initial surface undulation ($\delta(x_1) = \bar{\xi}_1 l \cos(2\pi x_1 / l)$, $\bar{\xi}_2 = 0$ with $\lambda_C{}^2 \bar{\xi}_1 = \pm 0.0005$). For the imperfect system the maximum compressive strain that can be imposed prior to the wrinkle becoming unstable is $\varepsilon^* = 1 - \lambda^*$.

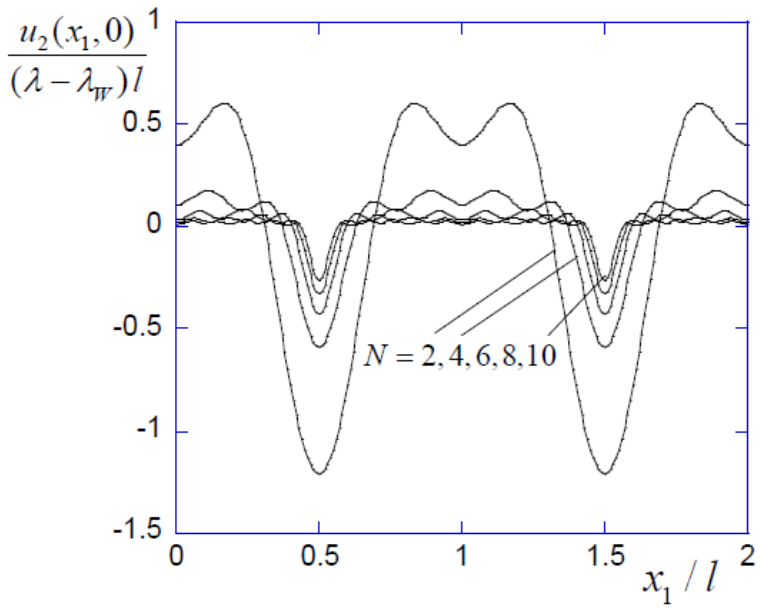

Fig. 3 The surface shape of the wrinkle mode of the perfect half-space as determined by the post-bifurcation analysis for a sequence of approximations with $N = 2,10$.

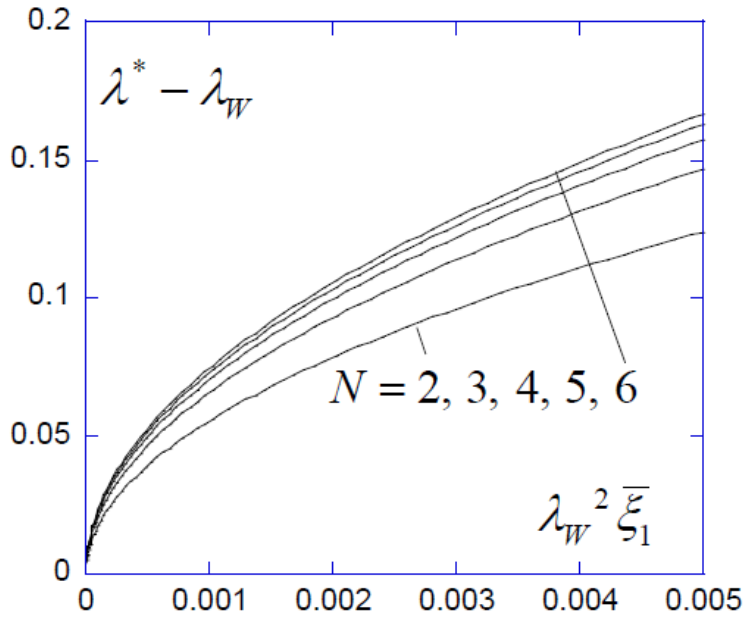

Fig. 4 Imperfection-sensitivity of wrinkling for sinusoidal imperfections. The maximum compressive strain that can be imposed given the normalized imperfection amplitude, $\overline{\xi}_1$, is associated with the stretch λ^*. Applicable for all λ_3 with λ_w given by (1.1).

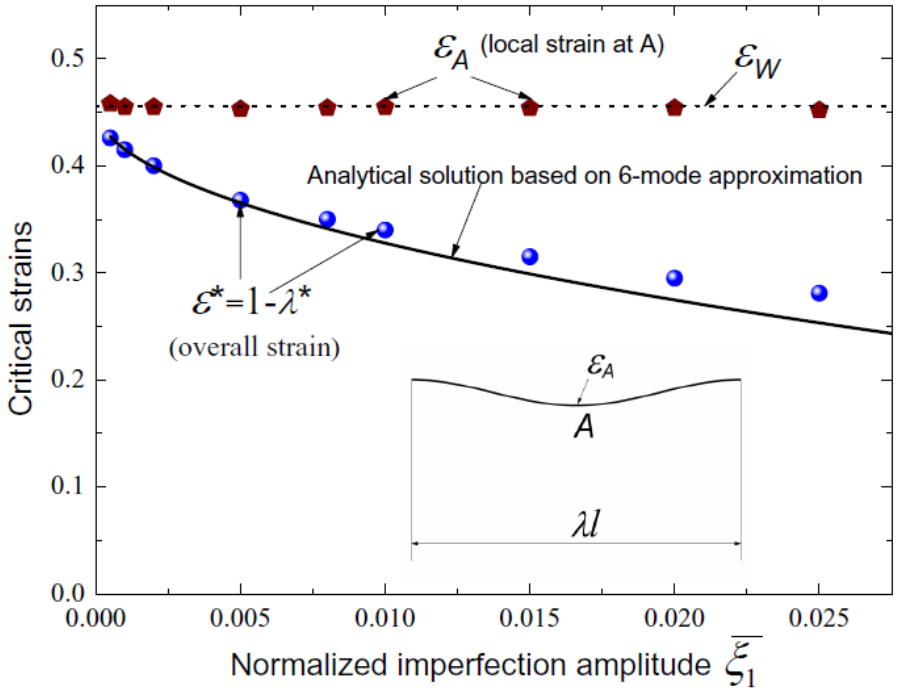

Fig. 5 Imperfection-sensitivity for the sinusoidal imperfection as predicted by the numerical simulations compared with the asymptotic analytical results. Finite element results in plane strain for the overall compressive strain at which the wrinkle becomes unstable, ε^*, and for the corresponding local compressive strain at the deepest point of the wrinkle, ε_A. Two important observations can be noted. Very small initial imperfections dramatically reduce the overall strain at instability so much so that an imperfection with amplitude less than one hundredth of its wavelength reduces the strain at instability to below the creasing strain (1.2). Secondly, instability is associated with the local compressive strain at A attaining the wrinkling strain, $\varepsilon_W = 0.456$.

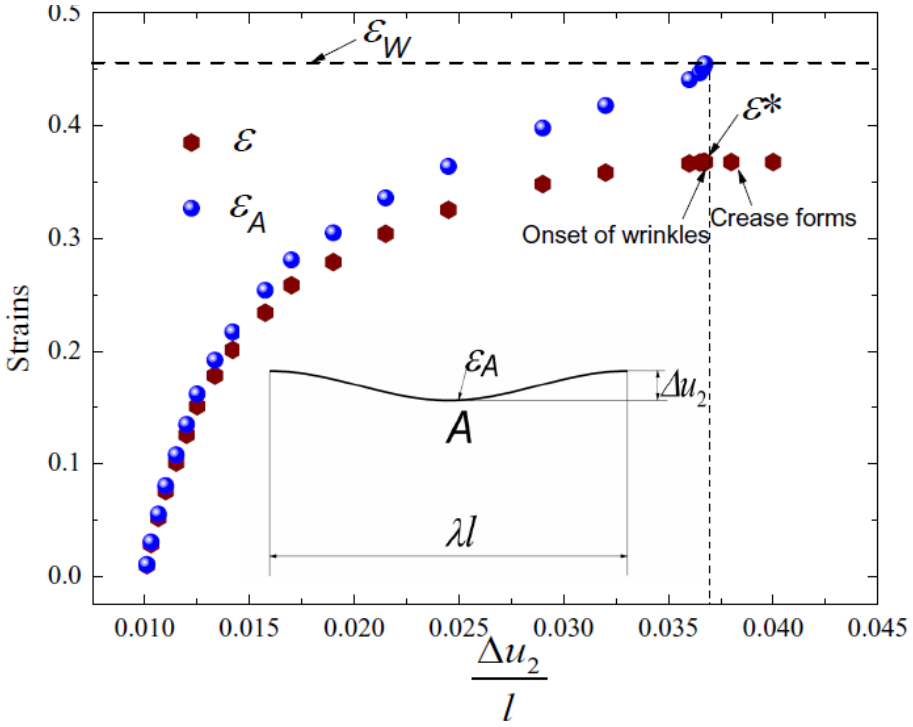

Fig. 6 The overall compressive strain, ε, and the local compressive strain, ε_A, at the deepest point on the surface as a function of the normalized surface height difference for the sinusoidal imperfection with $\bar{\xi}_1 = 0.005$. Both $\varepsilon_A = \varepsilon_W$ and attainment of a maximum of the overall compressive strain occur at the point of instability, to a high approximation.

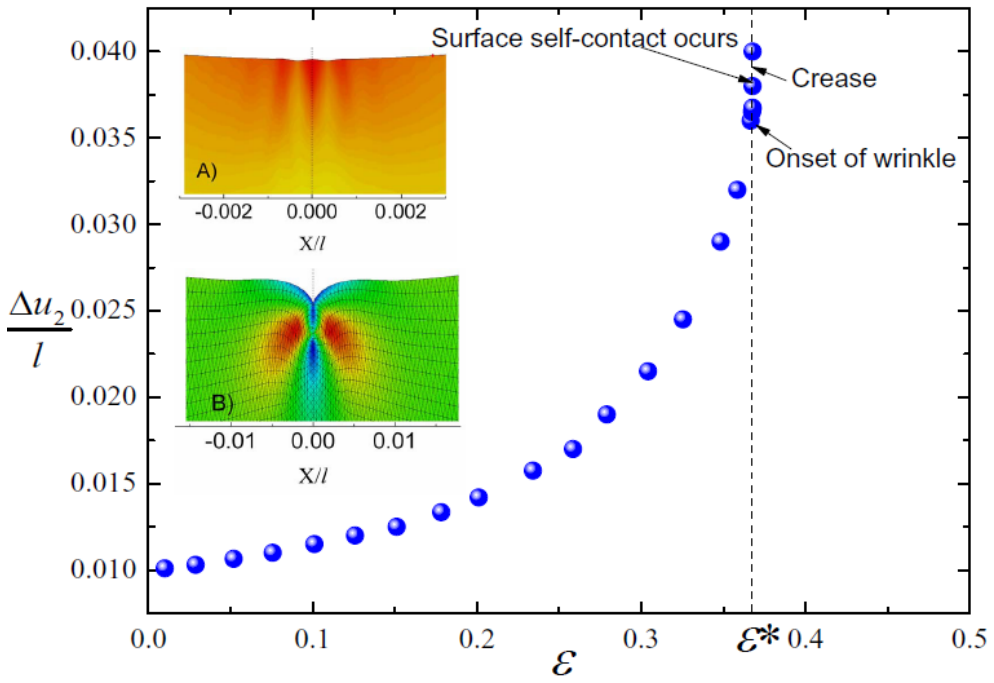

Fig. 7 Details of the development of the wrinkle and the formation of the crease for a sinusoidal imperfection with $\bar{\xi}_1 = 0.005$. The onset of instability (A) occurs when small scale wrinkling occurs at the minimum point on the surface at the overall strain, ε^*. With overall strain held constant, the crease develops in (B). The wrinkle becomes dynamically unstable when the overall strain attains ε^* and would collapse dynamically into the crease. The pseudo-dynamic algorithm used in the numerical simulations enable the transition to occur in a controlled manner. In the inserts, (A) and (B), X denotes the horizontal distance measured in the deformed state.

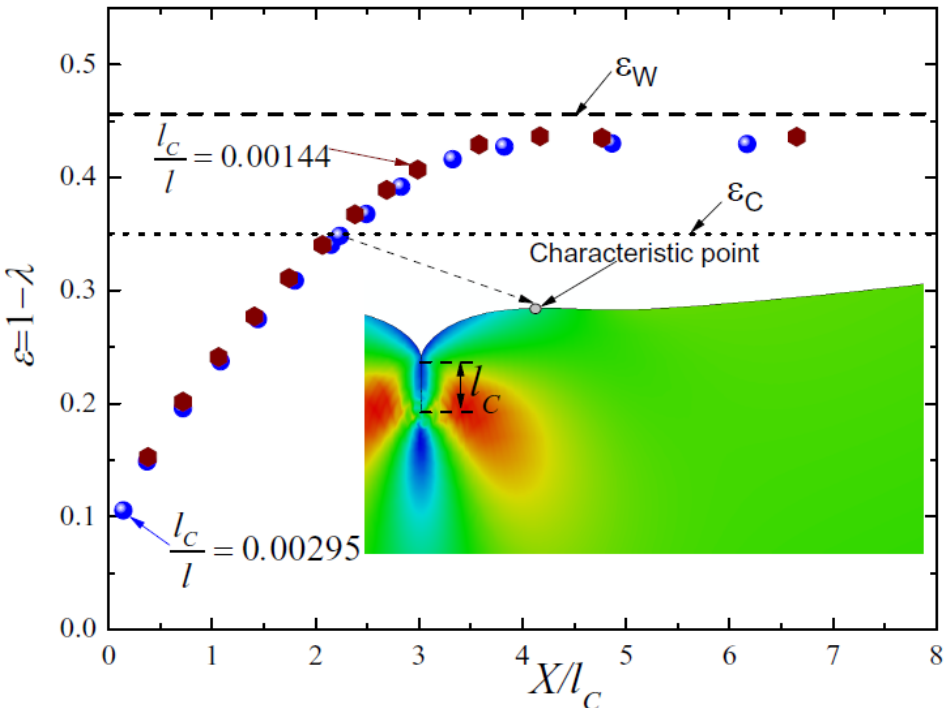

Fig. 8 Compressive strain distribution at the surface in the vicinity of the crease for a half-space with a sinusoidal imperfection with amplitude $\bar{\xi} = 0.005$ for two crease depths. X denotes the horizontal distance measured in the deformed state. A characteristic point on the surface, $X \simeq 2.3 l_C$, is noted where the strain equals the crease strain, ε_C. At this point, to a good approximation, the surface curvature switches from concave to convex. At distances $X < 2.3 l_C$ the strain at the surface is less than ε_C.

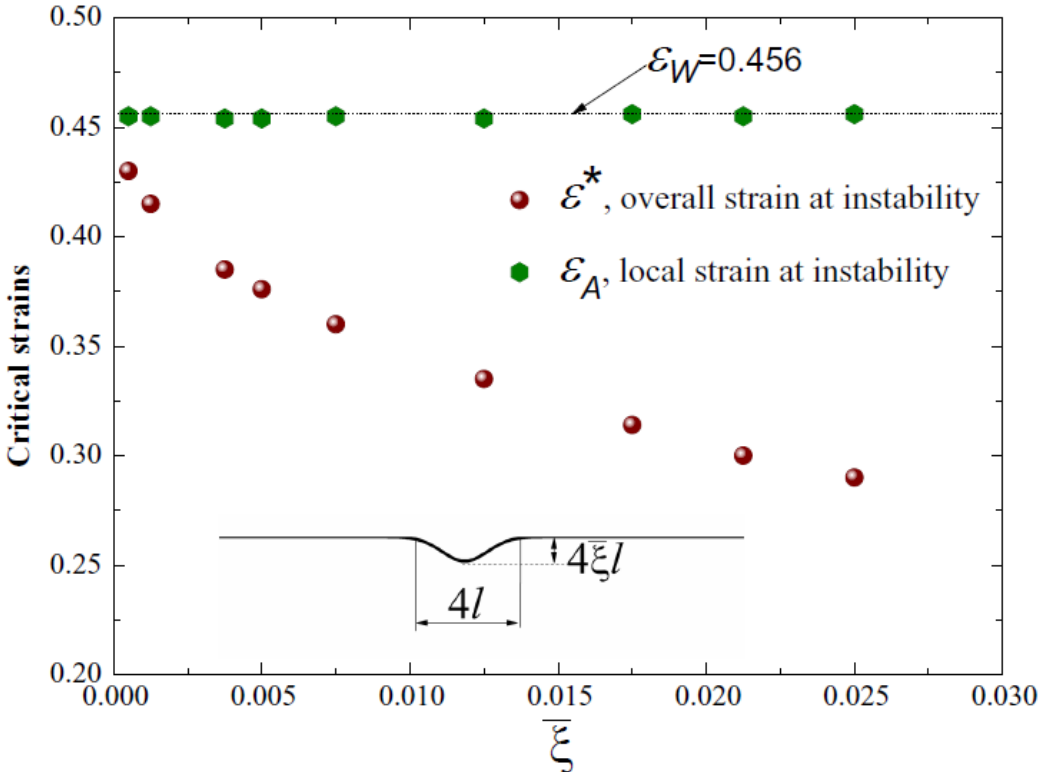

Fig. 9 Local and overall compressive strains at the wrinkling instability in plane strain for the exponential imperfection. The imperfection-sensitivity for this imperfection is similar to that for the sinusoidal imperfection.